Title

WRF simulation of downslope wind events in coastal Santa Barbara County

Authors

Cannon, Forest
Carvalho, Leila MV
Jones, Charles
et al.

Publication Date

2017-07-01

DOI

10.1016/j.atmosres.2017.03.010

Peer reviewed

Atmospheric Research 191 (2017) 57–73

Contents lists available at ScienceDirect

Atmospheric Research

journal homepage: www.elsevier.com/locate/atmosres

WRF simulation of downslope wind events in coastal Santa Barbara County

Forest Cannon [a,b,*], Leila M.V. Carvalho [a,b], Charles Jones [a,b], Todd Hall [c], David Gomberg [c], John Dumas [c], Mark Jackson [c]

[a] Department of Geography, University of California Santa Barbara, USA
[b] Earth Research Institute, University of California Santa Barbara, USA
[c] National Oceanic and Atmospheric Administration, National Weather Service, Los Angeles/Oxnard Weather Forecast Office, USA

ARTICLE INFO

Article history:
Received 13 June 2016
Received in revised form 6 March 2017
Accepted 9 March 2017
Available online 10 March 2017

Keywords:
Downslope winds
WRF
Mesoscale modeling
Southern California
Fire hazards
Sundowner winds

ABSTRACT

The National Weather Service (NWS) considers frequent gusty downslope winds, accompanied by rapid warming and decreased relative humidity, among the most significant weather events affecting southern California coastal areas in the vicinity of Santa Barbara (SB). These extreme conditions, commonly known as "sundowners", have affected the evolution of all major wildfires that impacted SB in recent years. Sundowners greatly increase fire, aviation and maritime navigation hazards and are thus a priority for regional forecasting. Currently, the NWS employs the Weather Research Forecasting (WRF) model at 2 km resolution to complement forecasts at regional-to-local scales. However, no systematic study has been performed to evaluate the skill of WRF in simulating sundowners.

This research presents a case study of an 11-day period in spring 2004 during which sundowner events were observed on multiple nights. We perform sensitivity experiments for WRF using available observations for validation and demonstrate that WRF is skillful in representing the general mesoscale structure of these events, though important shortcomings exist. Furthermore, we discuss the generation and evolution of sundowners during the case study using the best performing configuration, and compare these results to hindcasts for two major SB fires. Unique, but similar, profiles of wind and stability are observed over SB between case studies despite considerable differences in large-scale circulation, indicating that common conditions may exist across all events. These findings aid in understanding the evolution of sundowner events and are potentially valuable for event prediction.

1. Introduction

The Santa Barbara (SB) region of California is characterized by unique topography. The Santa Ynez Mountains, spanning a length of about 100 km and oriented approximately east-west with elevations >1200 m, rises abruptly from a narrow coastal plain. Among the most significant weather events affecting coastal areas of SB County are late afternoon-to-nighttime episodes of gusty downslope surface winds accompanied by rapid increases in temperature and decreases in relative humidity, commonly known as 'Sundowners'. Gale winds, relative humidity below 15% and temperatures above 35 °C (95 °F) are not uncommon during Sundowner events, even during the winter (Blier, 1998).

Sundowner events have played a significant role in the evolution of all major fires that have affected SB in recent years, including the Painted Cave (1990), Gap (2008), Tea (2008), and Jesusita (2009), and have been responsible for millions of dollars in property loss and significant impacts to the environment. The cities of Santa Barbara and Goleta, the largest in the County (91,196 and 30,525 inhabitants, respectively) are largely exposed to wildfire hazards with most of the population living in a narrow zone between the mountains and the ocean. Sundowners are also a major concern for aviation and maritime navigation, especially for small crafts. In one of the few studies that specifically investigate Sundowner events, Blier (1998) examined a number of physical processes and synoptic conditions associated with sundowners. It was found that significant perpendicular flow over the Santa Ynez Mountains' ridgeline is present in all instances such that the prevailing flow in the vicinity of SB is offshore (northerly), eroding the marine influence that typically exists. Local warming is largely explained by adiabatic descent from the above ridge-top level associated with mountain wave development and, to a lesser extent, the greater diurnal heating enabled in the absence of the cool onshore winds (sea breeze).

Strong, warm and dry downslope winds that occur on the lee side of the mountains, such as sundowners, are generically defined as "foehn

* Corresponding author at: Dept. of Geography, University of California, Santa Barbara, Santa Barbara, CA 93106, USA.
E-mail address: fcannon@geog.ucsb.edu (F. Cannon).

http://dx.doi.org/10.1016/j.atmosres.2017.03.010
0169-8095/

winds" (Brinkman, 1971). The dynamics of strong downslope winds and mountain waves have been described in numerous studies based on observations and modeling (e.g., Klemp and Lilly, 1975; Smith, 1979, 1985; Durran, 1990; Grubisic and Billings, 2007, 2008; Jiang and Doyle, 2008; Lawson and Horel, 2015; among others). The basic conditions necessary for the amplification of mountain waves and the occurrence of windstorms are: the stability of the air approaching the mountains, the speed of the air flow over the mountain, and the topographic characteristics of the underlying terrain (e.g. Durran, 1990). Though there are numerous types of downslope winds related to unique combinations of these mechanisms, previous work has shown that conditions favoring the development of windstorms generally arise from fundamentally similar processes, which can be identified through metrics such as the Froude Number, Richardson Number and Scorer Parameter (Durran, 2003). The Froude number, defined as the ratio of kinetic energy of the flow to the potential energy required to rise over the mountain (Holton, 2004), can be used to identify when conditions favor the development of mountain waves. Furthermore, the Scorer Parameter, which identifies vertical profiles of wind and stability that reflect vertically propagating wave energy above the mountaintop back to the surface (Scorer, 1949), can be used to identify when mountain waves will generate surface windstorms (e.g. Doyle and Shapiro, 1999).

Among downslope wind events, including sundowners, forcing mechanisms vary on an event-by-event basis on account of changes in the profile of atmospheric stability and winds. Furthermore, the criterion for producing downslope windstorms in a particular region can be met by a variety of synoptic conditions. The complex behavior of downslope winds elucidate the need for a dense network of instruments, including ones that can measure atmospheric conditions above the surface, to properly characterize their behavior, and reveal challenges in modeling the phenomenon (Doyle et al., 2011). While large-scale synoptic conditions create the background conditions necessary for the development of downslope flow, the evolution of the event depends on interactions with local topography on scales that vary from kilometers to the scale of the turbulence (e.g., Chow et al., 2012). Consequently, mesoscale models with horizontal resolution on the order of a few hundred meters (e.g. Grubisic and Billings, 2008) are often necessary to adequately simulate the evolution and structure of observed mountain waves.

The Los Angeles/Oxnard NWS office (NWS/LOX) relies in part on Weather Research and Forecasting (WRF) model simulations to complement their Santa Barbara forecast of sundowners. Our research presents the first thorough study of the efficacy of WRF in representing a collection of sundowner events, and discusses their dynamical evolution based on model output. Here, simulations are interpreted using general mountain wave theory, including quantifiable metrics such as the Richardson Number and Scorer Parameter (Scorer, 1949; Durran, 1990, 2003). Although downslope winds in the vicinity of SB are considered among the most important fire weather hazards in Southern California, dynamical and physical mechanisms associated with these events, including their synoptic-to-mesoscale characteristics, remain relatively unexplored. The primary goals of this research are: 1) to test the ability of WRF in simulating the evolution of sundowner events based on available observations, and 2) to improve understanding of the dynamical processes that generate sundowners, at high spatiotemporal resolution, both at the surface and above the mountaintop.

The manuscript is divided into eight sections. Section 2 details the data used in the study. Section 3 introduces the case-study sundowner event, justifies its selection, and gives a synoptic overview of the event. Section 4 details the different WRF configurations that were tested and Section 5 explains the sensitivity experiment results. The dynamics of the selected sundowner event are investigated in Section 6, using the best performing model configuration from Section 5. Section 7 compares the dynamics of the case-study sundowner event with two separate sundowner events that were responsible for major wildfires in Santa Barbara, and Section 8 summarizes the manuscript's key findings.

2. Data

2.1. In-situ data

Hourly data from 26 in-situ stations located throughout Southern California and offshore are employed in this study. Station data was gathered from NWS stations, Remote Automatic Weather Stations (RAWS), and National Oceanic and Atmospheric Administration – National Data Buoy Center (NDBC) buoys. The principal characteristics of the stations—altitude, coordinates and management agency—are detailed in Table 1, and their locations, along with a reference map of the study region, are shown in Fig. 1. Here, we consider temperature, relative humidity, wind speed and direction, and pressure (where available) for the period 0z Apr. 23, 2004–0z May 4, 2004 (UTC). It is important to note that NOAA, NWS and RAWS station data each come from unique instrumentation and adhere to slightly different recording standards. In addition to station data, we utilize data from twice-per-day radiosonde launches at Vandenberg Air Force Base (Fig. 1; Station 6) for WRF validation of vertical profiles.

2.2. Reanalyses

Climate Forecast System Reanalysis (CFSR) data, from the National Centers for Environmental Prediction (Saha et al., 2010), are used to investigate the large-scale dynamical environment during the study period, and provides initial and lateral boundary conditions to Weather Research and Forecasting Model (WRF) simulations. CFSR is available at 6-hourly 0.5° horizontal-resolution for the period 1979–2013. CFSR was chosen on account of its model coupling, spatial resolution, and modern data assimilation system (Saha et al., 2010). Analysis of geopotential height, omega, wind, moisture, and temperature are performed at 500-hPa with daily temporal resolution.

Table 1
Index of station names, latitude, longitude, elevation and collecting agency for the 26 meteorological stations shown in Fig. 1.

Stations	Elev. (m)	Lon.	Lat.	Agency
1. Montecito Hills	494	−119.694	34.461	RAWS
2. Santa Barbara Airport	3	−119.844	34.426	NWS
3. Los Prietos	299	−119.791	34.544	RAWS
4. Santa Rosa Island	391	−120.079	33.980	RAWS
5. Lompoc Airport	30	−120.467	34.677	NWS
6. Vandenberg Air Force Base	310	−120.486	34.759	RAWS
7. Figueroa Mountain	970	−120.007	34.734	RAWS
8. Santa Maria Airport	78	−120.449	34.900	NWS
9. Arroyo Grande	319	−120.393	35.197	RAWS
10. San Luis Obispo Airport	63	−120.636	35.236	NWS
11. Carrizo Plain Natl. Mnmt.	759	−119.773	35.097	RAWS
12. Bakersfield Airport	155	−119.057	35.437	NWS
13. Sandberg	1378	−118.724	34.744	NWS
14. Lancaster Airport	715	−118.219	34.741	NWS
15. Del Valle (Castaic)	390	−118.667	34.430	RAWS
16. Burbank Airport	222	−118.365	34.200	NWS
17. Los Angeles Intl. Airport	38	−118.389	33.938	NWS
18. Leo Carrillo St. Park	15	−118.936	34.045	RAWS
19. Pt. Mugu Naval Base	3	−119.122	34.124	NWS
20. Lake Casitas	195	−119.371	34.408	RAWS
21. Ozena	1125	−119.354	34.682	RAWS
22. E. Santa Barbara Channel Buoy	0	−119.853	34.252	NDBC
23. W. Santa Barbara Channel Buoy	0	−120.477	34.265	NDBC
24. Point Arguello Buoy	0	−121.019	34.956	NDBC
25. South Santa Rosa Buoy	0	−120.212	33.674	NDBC
26. Santa Monica Basin Buoy	0	−119.053	33.749	NDBC

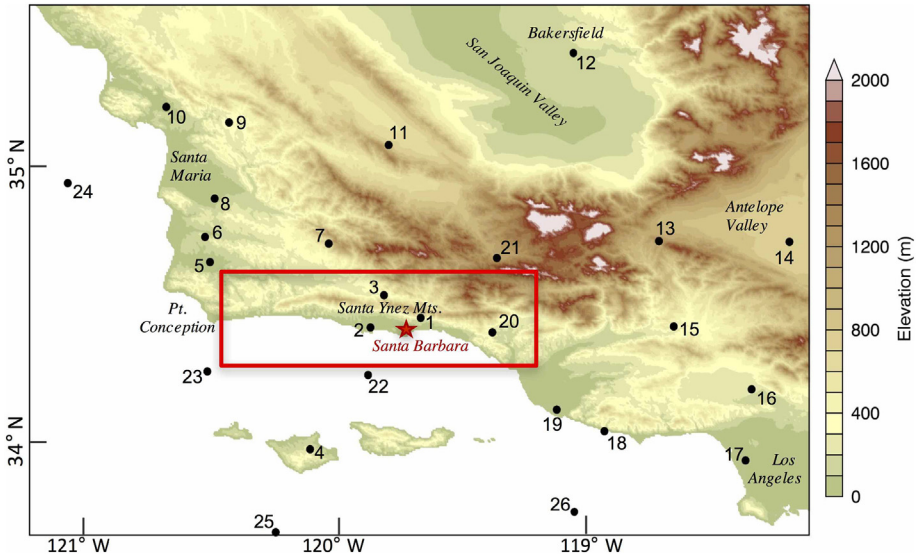

Fig. 1. Southern California study domain, corresponding to the inner domain of the WRF simulation. Station locations are identified by number, corresponding to Table 1. Red box indicates study region focus area within WRF inner domain, including the Santa Barbara coastal plain and Santa Ynez Mountains, where "sundowner" events are typically observed. (For interpretation of the references to color in this figure legend, the reader is referred to the web version of this article.)

2.3. Satellite observations

Moderate Resolution Imaging Spectroradiometer (MODIS) data from both the Terra and Aqua satellites are additionally used to validate spatial patterns of surface temperature (MOD/MYD11A1; Wan, 1999) at 1 km resolution during sundowner events. During daytime, temperature estimates from radiance retrievals are prone to biases based on surface exposure, land cover type and atmospheric conditions, typically resulting in the overestimation of temperature. Contrastingly, at night MODIS derived land surface temperatures compare well with station measurements above the surface (Zhang et al., 2014).

Advanced Very High Resolution Radiometer (AVHRR) sea surface temperature (SST) data (Casey et al., 2010) are used for model validation over the ocean. Additionally, AVHRR are used to modify the surface boundary conditions in several WRF simulation sensitivity tests.

3. Description of the event

3.1. Local influence in Santa Barbara

The Apr. 23–May 4, 2004 event was selected for study based on the number of consecutive nights classified by the NWS/LOX as "sundowner" events (Personal Communication). The following criteria have been used by the NWS/LOX to classify the events (Dorman and Winant, 2000): (1) sustained winds ≥ 25 mph (11.2 m/s), (2) wind gusts ≥ 35 mph (15.6 m/s), and (3) a northerly component in the wind direction. In this context "sustained" means the 2-minute average wind speed at the Montecito Hills RAWS stations (~6.0 m tower height). While these thresholds are significant for fire weather forecasts, they do not differentiate events according to mechanisms responsible for the strong winds, nor do they account for the impacts of temperature and RH, or for the seasonality of these episodes. Moreover, given the complexity of topography and proximity to the ocean, these thresholds may represent different percentiles of the wind distribution at each individual station.

The selected events investigated here were associated with very low relative humidity, which in combination with strong and gusty winds were of great relevance for fire weather hazards in the region. Specifically, the nights of April 24, 27, 28 and May 2 and 3 experienced hourly-averaged northerly winds at the Montecito Hills station (station 1 in Fig. 1) that exceeded 12 m/s (~25 mph), with gusts >16 m/s (~35 mph), and relative humidity values below 15%. The Montecito Hills station is critical to assessing sundowner activity because of its location in a particularly fire-prone area of the Santa Barbara foothills. Though a fire did not occur during this period, the conditions spurred the NWS/LOX to issue a "Red-Flag Warning", which is a forecast warning to inform area firefighting and land management agencies that conditions favoring extreme fire danger and/or fire behavior are either imminent or are occurring. The criteria for Red-Flag Warnings (Table 2) indicate the NWS emphasis on strong winds and dry atmospheric conditions for fire hazard forecasting.

3.2. Large-scale event conditions

The synoptic conditions that prevailed during this event, and ultimately led to the local sundowner conditions, are displayed in Fig. 2. For one week prior to the peak of sundowner activity in the early mornings of April 27th and 28th, a strong blocking high developed west of the California coast, exhibiting 500 hPa geopotential height in excess of 5800gpm and sea level pressure in excess of 1030 hPa. Anticyclonic flow on the eastern side of the surface high produced N/NW winds along the coast, while the regional high pressure also allowed for considerable diabatic heating of inland areas. Late on the 28th through the 30th, a weak shortwave trough from NW Canada dipped southward into the Great Basin. On the 30th, the region of low pressure moved east as a cutoff low and a second intense ridge became established over the West Coast. Sundowner conditions were again observed in the morning hours of the 2nd and 3rd of May, during prevailing high pressure. Though not all downslope wind events in SB develop from similar large-scale conditions, the synoptic features described here were

Table 2
National Weather Service "Red Flag" warning criteria for severe fire weather hazards forecasting.

Red flag warning criteria (with critical fuels)	
Criteria 1	RH ≤ 10% with sustained wind ≥ 15 mph (6.7 m/s) and/or frequent gusts ≥ 25 mph (11.2 m/s)
Criteria 2	RH ≤ 15% with sustained wind ≥ 25 mph (11.2 m/s) and/or frequent gusts ≥ 35 mph (15.6 m/s)
Criteria 3	Widespread and/or significant dry lightning
Criteria 4	Other (forecaster discretion)

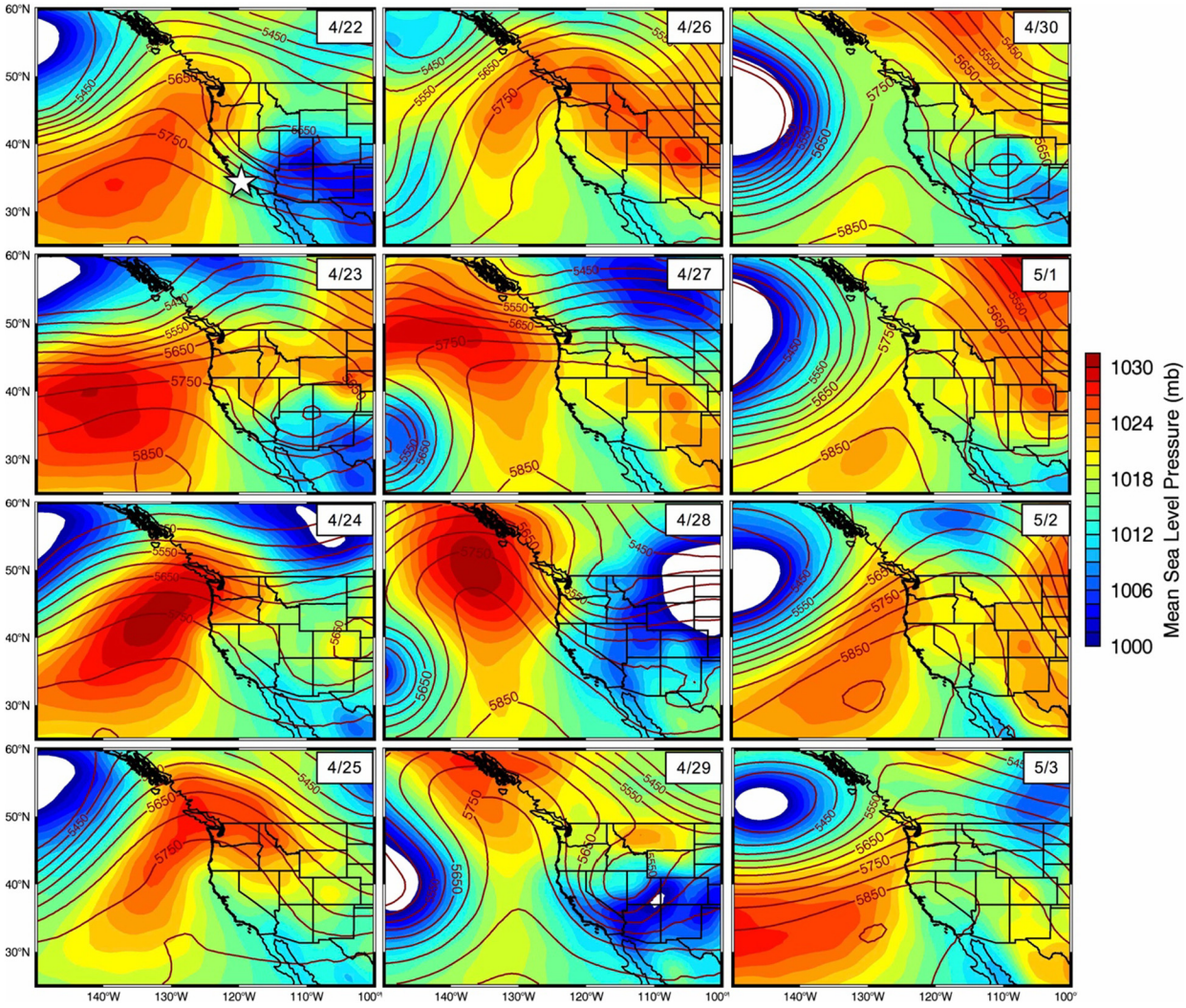

Fig. 2. Daily-averaged CFSR mean sea-level pressure (color; hPa) and 500-hPa geopotential height (contours; gpm) for the 11-day case study. The white star in the top left panel indicates the approximate location of the study region. (For interpretation of the references to color in this figure legend, the reader is referred to the web version of this article.)

representative of the development of events associated with very low relative humidity and therefore relevant for fire weather hazards.

4. Methodology: model configuration

The 11-day case study spanning Apr. 23, 2004 to May 4, 2004 was simulated using version 3.7.1 of the Advanced Research Weather and Forecasting (WRF-ARW, hereafter WRF) model (Skamarock et al., 2008). The 265-hour simulation was performed using three nested domains with one-way interaction (18 km, 6 km and 2 km spatial resolution, respectively), on a Mercator projection, and using 41 vertical levels. The inner domain is displayed as the spatial extent of Fig. 1. Initial and lateral boundary conditions were provided by CFSR. Three configurations were tested in this study. The parameterization schemes for the three different configurations are listed in Table 3. Model configuration-1 (WRF-1) employs parameterization schemes that have been used in

Table 3
Parameterization schemes employed for the three WRF configurations that were tested.

Parameterizations employed in tested configurations			
Configuration name	WRF-1	WRF-2	WRF-3
Microphysics	WRF Single Moment 5-Class (Hong et al., 2004)	WRF Single Moment 5-Class (Hong et al., 2004)	Morrison 2-Moment (Morrison et al., 2009)
Surface layer	Revised MM5 Monin-Obukhov (1) Beljaars et al. (1994)	Revised MM5 Monin-Obukhov (Beljaars et al., 1994)	Mellor-Yamada-Nakanishi-Niino (Nakanishi and Niino, 2009)
Land surface	Unified Noah (Tewari et al., 2004)	Unified Noah (Tewari et al., 2004)	Unified Noah (Tewari et al., 2004)
Longwave radiation	Rapid Radiative Transfer Model for GCMs (Iacono et al., 2008)	Rapid Radiative Transfer Model for GCMs (Iacono et al., 2008)	Rapid Radiative Transfer Model (Mlawer et al., 1997)
Shortwave radiation	Rapid Radiative Transfer Model for GCMs (Iacono et al., 2008)	Rapid Radiative Transfer Model for GCMs (Iacono et al., 2008)	Dudhia (Dudhia, 1989)
Boundary layer	Yonsei University (Hong et al., 2006)	Mellor-Yamada-Nakanishi-Niino (Nakanishi and Niino, 2009)	Mellor-Yamada-Nakanishi-Niino (Nakanishi and Niino, 2009)
Cumulus	Kain Fritsch (outer domain only, Kain, 2004)	Kain Fritsch (outer domain only, Kain, 2004)	Kain Fritsch (outer domain only, Kain, 2004)

previous studies focused on winter precipitation events in California, for which WRF has been more thoroughly tested than fire weather conditions (e.g. Caldwell et al., 2009; Chin et al., 2010; Smith et al., 2010; Dulière et al., 2011).

Since the focus of this study is on dry conditions, we tested two additional configurations. Model configuration-2 (WRF-2) is a sensitivity test for which we replaced the boundary layer configuration used in WRF-1 with Mellor-Yamada-Nakanishi-Niino (MYNN; Nakanishi and Niino, 2009). Previous studies evaluating WRF performance in Southern California have identified PBL schemes as a primary source of error (Huang et al., 2013; Scarino et al., 2014). These studies established that available parameterization schemes produce significant differences in PBL height compared to large-eddy simulated (Huang et al., 2013) and light detection and ranging (LIDAR) estimates (Scarino et al., 2014), and that these issues are exacerbated near the coastal zone, which adversely affects the simulation of sundowner wind influence over SB (communication with NWS LA/Oxnard office). The MYNN PBL parameterization was adopted in WRF-2 because of the reported improvement of the turbulent length scale that realistically increases with decreasing stability, and the improvement of the expression for stability functions for momentum and heat. Huang et al. (2013) also demonstrated this to be the "best" performing PBL parameterization for a number of case studies focused on representing the marine layer in coastal California, though none of the tested parameterizations were ideal.

A third configuration (WRF-3), using the PBL parameterization from WRF-2 but with different microphysics, surface layer, longwave and shortwave radiation schemes, was also tested. The WRF-3 configuration combines modifications suggested in Walton et al. (2015) and the experience of the NWS/LOX in operationally forecasting sundowner events using WRF. This is the configuration that was used by the NWS/LOX operational forecasts at the time of this study. Additionally, we discuss sensitivity tests with improved horizontal resolution (1 km inner domain) and various SST forcing schemes, including time-varying SST and SST from the Advanced Very High Resolution Radiometer (AVHRR) as the lower boundary initial condition (WRF-3/A). A single simulation with improved vertical resolution (61 levels) was also tested and although minor differences were observed above the mountaintop during sundowner events, it was not possible to evaluate these given the lack of observations above the surface.

5. Sensitivity experiments and validation

The establishment of an optimal WRF configuration for sundowner event forecasting is complicated by the lack of observations for validation. In this study, validation is limited to 26 surface stations with hourly records (Fig. 1), twice-per-day surface temperature estimates from satellites, and one twice-per-day radiosonde at Vandenberg Air Force Base (Fig. 1; Label 6). Unfortunately, there are no observational data for validating the vertical profile of winds over the Santa Ynez Mountains and SB during these events.

Table 4
Average Pearson correlation coefficient of station data with the corresponding WRF grid cell over the 11-day study period, Apr. 23–May 4, 2004 for all available stations in the study domain. WRF temperature and relative humidity are taken from the 2 m level. Wind speed is taken from 10 m and pressure is taken from the surface. The last column "Average" is the mean of all four variables.

Correlation of WRF configurations with station data					
Configuration	Temperature	R. humidity	Wind speed	Pressure	Average
WRF-1	0.84	0.70	0.57	0.94	0.75
WRF-2	0.84	0.70	0.56	0.95	0.74
WRF-3	0.85	0.70	0.62	0.94	0.76
WRF-3/A	0.83	0.72	0.62	0.94	0.76

5.1. Validation: stations

Table 4 lists correlation values between the timeseries of stations and the corresponding WRF gridpoints for temperature, relative humidity, wind and pressure at each hourly time step (265 h over 11 days) in each of the tested configurations. Among all variables validated in this study, pressure exhibits the highest correlation (0.94 or greater). WRF also simulates well the diurnal cycle of temperature at 2 m, with the majority of land-based stations registering 0.90 or greater, and each configuration's average correlation above 0.83. Coastal stations and buoys tended to have lower correlations, presumably on account of difficulties in simulating marine influence. Relative humidity was also generally well correlated for land stations, with values exceeding 0.75 at half of the stations in each of the configurations, and the remainder of stations generally above 0.5. Recorded wind speed at stations was not particularly well correlated with stations, though the WRF-3 configuration displayed the best relationship with observations ($r = 0.62$). Additionally, using AVHRR SST to modify WRF's initial conditions (WRF-3/A configuration) improved the simulation of coastal humidity, largely owing to a warm bias in the CFSR input that was corrected by incorporating the satellite data. Overall, the WRF-3/A configuration had the highest cumulative correlations for each tested variable, although the discrepancies between modeled and observed temperature, relative humidity and wind are large in comparison to the small differences across tested configurations. Continued analyses in this manuscript specifically focus on the WRF-3/A configuration.

Fig. 3 shows Google Earth imagery of the locations of two meteorological stations of interest (the Montecito Hills Station and the Santa Barbara Airport Station) and the size/location of the corresponding WRF grid cell. The location of these stations in reference to surrounding coastlines and complex topography illustrates reasons for discrepancies between observed and simulated conditions at these stations. Fig. 4 displays timeseries comparing the Montecito station and the corresponding WRF gridpoint from WRF-3/A. Additionally, a 3-day simulation employing 1 km horizontal resolution with the WRF-3/A configuration, which was performed to test model sensitivity to horizontal resolution, is displayed. The Montecito station is located in the foothills of the southern slope of the Santa Ynez Mountains, northeast of the city of Santa Barbara (Fig. 3). This particular location is considered extremely fire-prone and is thus our primary region of interest with respect to sundowner wind activity. The ability of WRF in simulating measured temperature, humidity and wind near the surface varies by location and prevailing meteorological conditions. For the Montecito station the relationship between model and observation is quite good. Temperature at 2 m is correlated with station temperature at 0.91, relative humidity at 0.91 and wind speed at 0.79 in the 2 km simulation. For the given station, WRF exhibits a smaller diurnal amplitude of temperature than observed, with a 2.3 °C cold bias in daytime temperatures that is responsible for a −0.5 °C difference in overall mean temperature. However, the good agreement between modeled and observed temperature at night during the peak of sundowner activity (indicated by the vertical black lines) is particularly encouraging. Relative humidity values observed at the Montecito station are typically very dry (generally below 20% during the period dominated by large-scale high pressure lasting from 4/23–4/29 and 5/1–5/4). The simulated relative humidity is approximately 5% higher during the same period. Also, the strong agreement between WRF 1 km and 2 km simulations for the Montecito Hills regions over the three overlapping days suggests that WRF cold bias does not significantly depend on the horizontal resolution. Similarly, increasing vertical resolution does not seem to improve the accuracy of the model in simulating the observed temperatures and relative humidity (not shown).

Fig. 4 also indicates good temporal agreement between modeled and observed wind speed, although a systematic negative bias of approximately 5 m/s during sundowner activity exists. For all records in which the observed wind speed exceeded 10 m/s (~22 mph), the

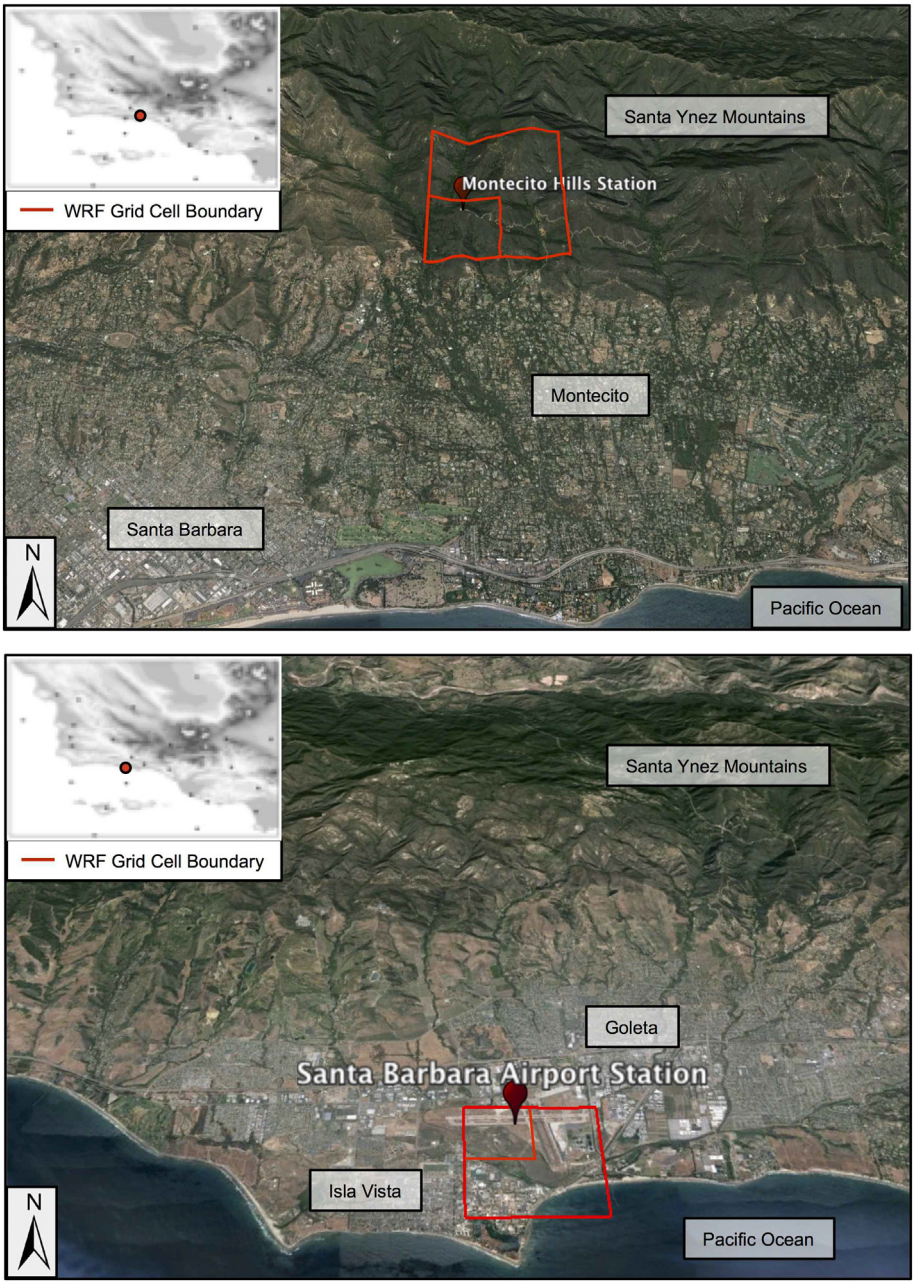

Fig. 3. Google Earth image of station location in Santa Barbara area. Red dot on grayscale map in upper left corner indicates station location in the study domain. Montecito Hills station is shown in the top panel and the Santa Barbara airport station is shown in the bottom panel. The large (small) red square represents the corresponding WRF grid cell in the 2 km (1 km) resolution simulation. (For interpretation of the references to color in this figure legend, the reader is referred to the web version of this article.)

average observed wind speed was 13.5 m/s (~30 mph) and the simulated wind speed for the corresponding gridpoint was 8.5 m/s (~19 mph). The direction of the wind during these events was almost uniformly N/NE in observations and simulation (not shown). During the peak of sundowner activity on April 27th at 3 AM, the WRF gridpoint corresponding to the Montecito station experienced hourly averaged winds from the NNE at 9.5 m/s (21.3 mph), temperature of 28.3 °C (~83 °F), and relative humidity of 11.5%. The station record showed average winds from the NNE at 15.2 m/s (34 mph) with gusts of 18.8 m/s (42 mph), temperature of 27.8 °C (82 °F) and relative humidity at 12%. The good agreement between simulated and observed values of temperature and relative humidity is remarkable considering the spatial resolution.

The discrepancy between modeled and observed wind speed during the event and throughout the simulation is of particular interest because of the importance of winds to fire weather forecasting. During sundowner events, winds are often highly variable, both spatially and temporally, posing a considerable challenge to forecasting the location and magnitude of the strongest winds, which is of utmost importance to firefighting agencies trying to position resources. It is not possible to state an exact reason for the discrepancy, though possible influences range from station siting to fundamental differences between wind measurements at 6 m elevation at the RAWS site and 10 m simulated wind that is extrapolated from the lowest model level. Overall, WRF appears to capture the temporal evolution of sundowner influence on the southern slope of the Santa Ynez Mountains throughout the simulation, indicating that the model is skillful in simulating the surface expression of sundowner events in regions of critical fire hazard. Furthermore, the NWS typically uses WRF to evaluate tendencies in variables of interest rather than their magnitude, understanding that WRF magnitudes are prone to biases.

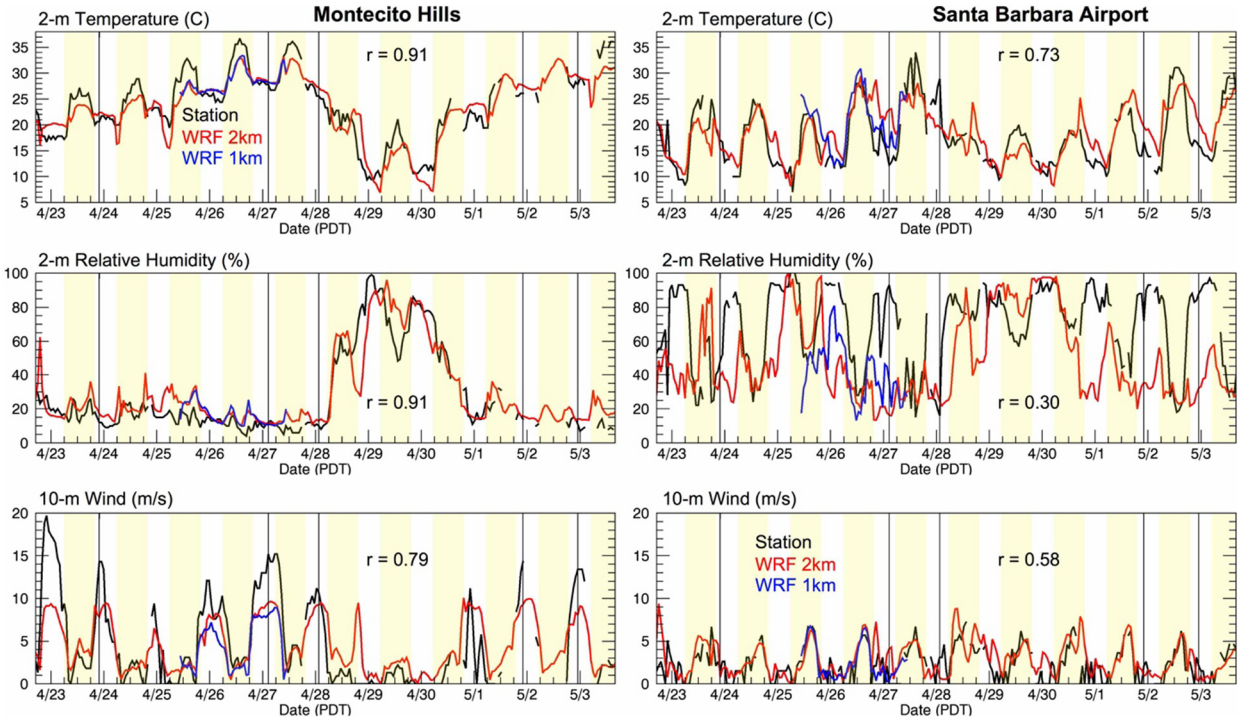

Fig. 4. Time series comparison of Montecito Hills station temperature relative humidity and wind with the corresponding WRF grid cell (left). Similar comparisons are shown for the Santa Barbara airport station (right). WRF timeseries appears in red. Correlation between timeseries is shown in each plot. The black lines indicate the time of the maximum observed wind speed at the Montecito Hills station for each night when conditions met the NWS "sundowner" criterion in Table 2. Yellow bars indicate daylight hours. (For interpretation of the references to color in this figure legend, the reader is referred to the web version of this article.)

Though the previous analyses support the capabilities of WRF as a fire-hazard forecasting tool, similar comparative analyses for other stations identify gross deficiencies in WRF's simulation of local meteorology, particularly at coastal stations. For example, comparison of temperature, relative humidity and wind between the Santa Barbara Airport station and the corresponding WRF gridpoint at 2 m indicates less agreement (Fig. 4). The Santa Barbara Airport is of particular interest for forecasting for aviation, which can experience significant hazards during sundowner events. Throughout the period simulated, sundowner events do not appear to strongly influence the referenced station, as nighttime wind speeds never exceed 5 m/s (~11 mph). However, early in the evening on April 26th (local time), WRF exhibited near-surface wind speed in excess of 7 m/s (~15 mph) from the north, indicating that the sundowner event that was experienced in the mountains was also influencing conditions at the airport. Though this often does occur, based on observations and local experience, during the particular event the simulated influence was in error. This discrepancy is further evidenced by the WRF temperature record, which shows an early evening spike in temperature and rapid decrease in relative humidity, both of which are not apparent in the observation record. The temporal evolution of humidity in WRF in comparison to observations reveals serious deficiencies in WRF's simulation of the coastal environment and marine layer, an issue that was previously documented by Huang et al. (2013). The NWS recognizes the simulation of the marine layer as a primary challenge in forecasting the downslope extent of sundowners (personal communication with the NWS).

The 1 km horizontal resolution simulation improved agreement between observed and modeled wind speeds, temperature and humidity at coastal stations (blue line in Fig. 4). It appears that the considerable fraction of the coarser 2 km resolution cell that overlaps the ocean surface negatively impacts the WRF simulation for the given point (Fig. 3). Despite the apparent benefit of increased horizontal resolution near the coast, differences between simulations in the mountains and inland were not appreciable. Surface temperature, humidity and winds in the 1 km simulation each had correlations >0.90 with the 2 km simulation at the Montecito Hills station. Furthermore, means and standard deviations of temperature, humidity and wind at the Montecito Hills station were nearly identical between different resolution simulations. Given the necessary computational resources to operationally perform simulations with horizontal resolution of 1 km over the same domain, we focus our discussion on the WRF-3/A configuration at 2 km resolution.

5.2. Validation: radiosonde

Over the majority of the domain there are no available observational data to evaluate WRF above the surface. The lone exception is the Vandenberg Air Force Base's twice-daily radiosonde (Station 6 in Fig. 1), which is beyond the influence of sundowner winds. The discrepancy between conditions at this site and in the region affected by sundowners is expected to be greatest at low levels and within the boundary layer. Fig. 5 displays the differences in temperature, mixing ratio, wind speed and wind direction, between the Vandenberg Air Force Base radiosonde observations and the corresponding WRF-3/A gridpoint data for the 0Z (5:00 PM PST) and 12Z (5:00 AM PST) soundings on each day of the simulation period (April 23rd - May 4th, 2004; 23 soundings). Radiosonde data was interpolated onto WRF's vertical grid for comparison. Only the lowest 5 km of the atmosphere are shown. "Bias" refers only to the differences observed over the 23 soundings and not a systematic model bias.

WRF temperature bias above 1 km is small, with a mean of <1 °C compared to radiosonde observations. However, within the lowest kilometer of the atmosphere, WRF exhibits a warm bias of several degrees, likely due to difficulties in simulating the frequent occurrence of an inland penetrating marine layer in this region. WRF also underestimates the observed mixing ratio in the lowest kilometer of the sounding, further emphasizing the influence of a poorly simulated marine layer.

WRF consistently underestimates observed wind speed and exhibits a negative bias of approximately 8 m/s (Fig. 5; bottom left). However, wind direction is generally well represented, and disagreement is limited to instances when the magnitude of the wind is small (Fig. 5, bottom

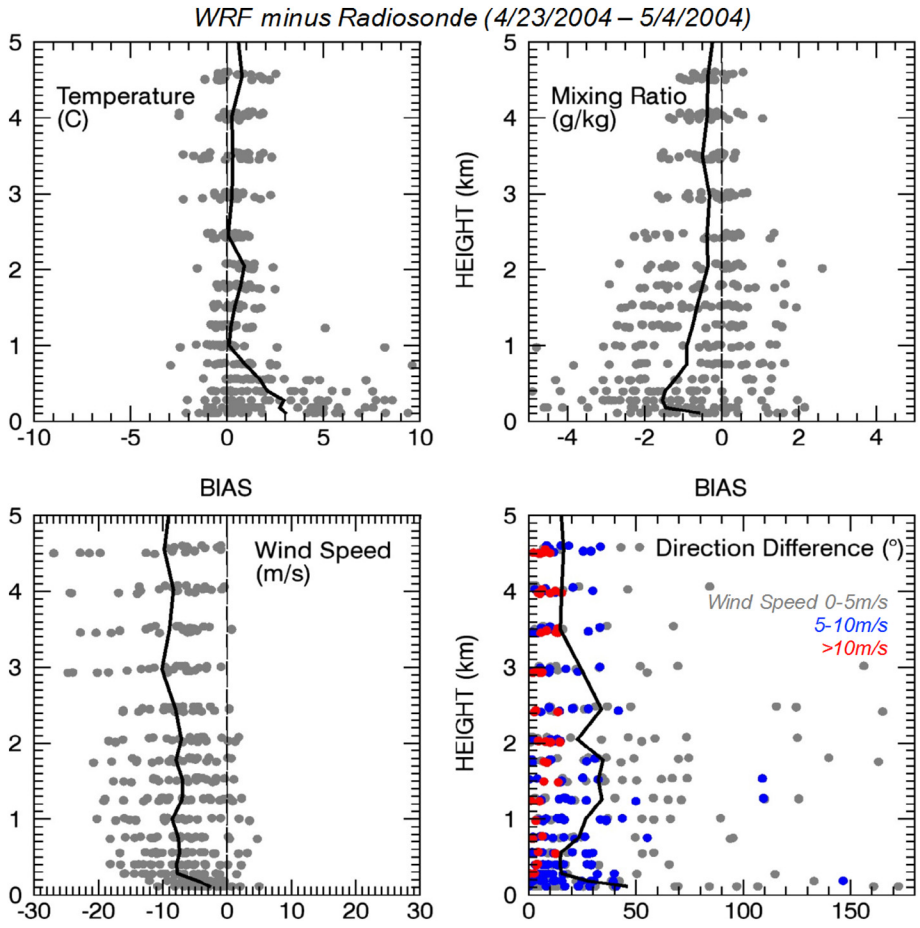

Fig. 5. Scatterplots of differences in temperature, mixing ratio wind magnitude and wind direction between the Vandenberg Air Force Base radiosonde observations and the corresponding WRF gridpoint for the 0Z (5:00 PM PST) and 12Z (5:00 AM PST) soundings on each day of the simulation period (April 23rd–May 4th, 2004). The black line in each panel indicates that variable's mean bias at each WRF vertical level. Only the lowest 5 km are shown. Colors in the bottom-right panel indicate WRF wind speed categories. (For interpretation of the references to color in this figure legend, the reader is referred to the web version of this article.)

right). When both the radiosonde and model wind speed exceed 10 m/s, the average difference in the direction of WRF and radiosonde winds at all levels is approximately 7°. Between 5 and 10 m/s, the difference is ~27° and for wind speeds below 5 m/s the difference is 63°. Differences between modeled and observed winds are somewhat height dependent, as winds above 3 km are generally stronger, exhibit a larger negative bias in magnitude and a smaller directional difference. The largest directional differences are found between 1 and 3 km, where considerable shear is observed (Section 6), and at the surface, although mean differences remain below 30°. This is important to note because velocity and directional shear in the large-scale cross-barrier wind appear influential in sundowner development (Section 6).

Although the Vandenberg sounding site is not ideally situated for validating WRF's simulation of sundowner conditions, these data aid in identifying bias in the profiles of temperature, moisture and wind. Above the boundary layer, these variables generally agree with observations, bolstering confidence in WRF's ability to simulate the meso-to-large scale features that lead to sundowner development, including changes in stability, and velocity and directional wind shear above the mountains, which are discussed in Section 6.

5.3. Validation: MODIS

The spatial structure of WRF skin temperature gradients is evaluated during the peak of the sundowner event on April 27th, and during the afternoon preceding the peak, using MODIS LST (Fig. 6). At 3 PM local time on the 26th, surface temperatures exhibit strong diabatic heating in inland valleys including the San Joaquin, Santa Ynez and Antelope valleys. Coastal areas and high elevations remain notably cooler. We recall that during daytime, temperature derived from radiance retrievals are prone to biases based on surface exposure, land cover type and atmospheric conditions, all of which affect radiative transfer and thus the efficacy of MODIS's algorithm. However, despite these issues, it is clear that the spatial pattern of surface temperature is very similar between satellite observation and WRF, and this is further evidenced in the nighttime LST scene. The most notable feature of the nighttime comparison is the high LST (~27 °C) observed over the southern slope of the Santa Ynez Mountains during the peak of the sundowner event in both MODIS and WRF.

5.4. Validation: summary

Overall, the limited validation that was possible in this study indicates that WRF (particularly the WRF-3/A configuration) properly simulates the evolution of near-surface temperature and wind at mesoscales over the entire domain during the studied event. Additionally, WRF's vertical profile of wind at the only available observation site exhibited a moderate negative bias in magnitude and good directional agreement with the radiosonde data. However, it is apparent that moisture is poorly represented in the coastal environment. In regions devoid of marine influence, the simulation of moisture during the studied period is greatly improved. On the southern slope of the Santa Ynez Mountains, where sundowner events generate considerable fire danger, WRF seems to accurately represent local meteorology throughout the simulation, including during sundowner activity. However, the few observational data available for validation are a significant

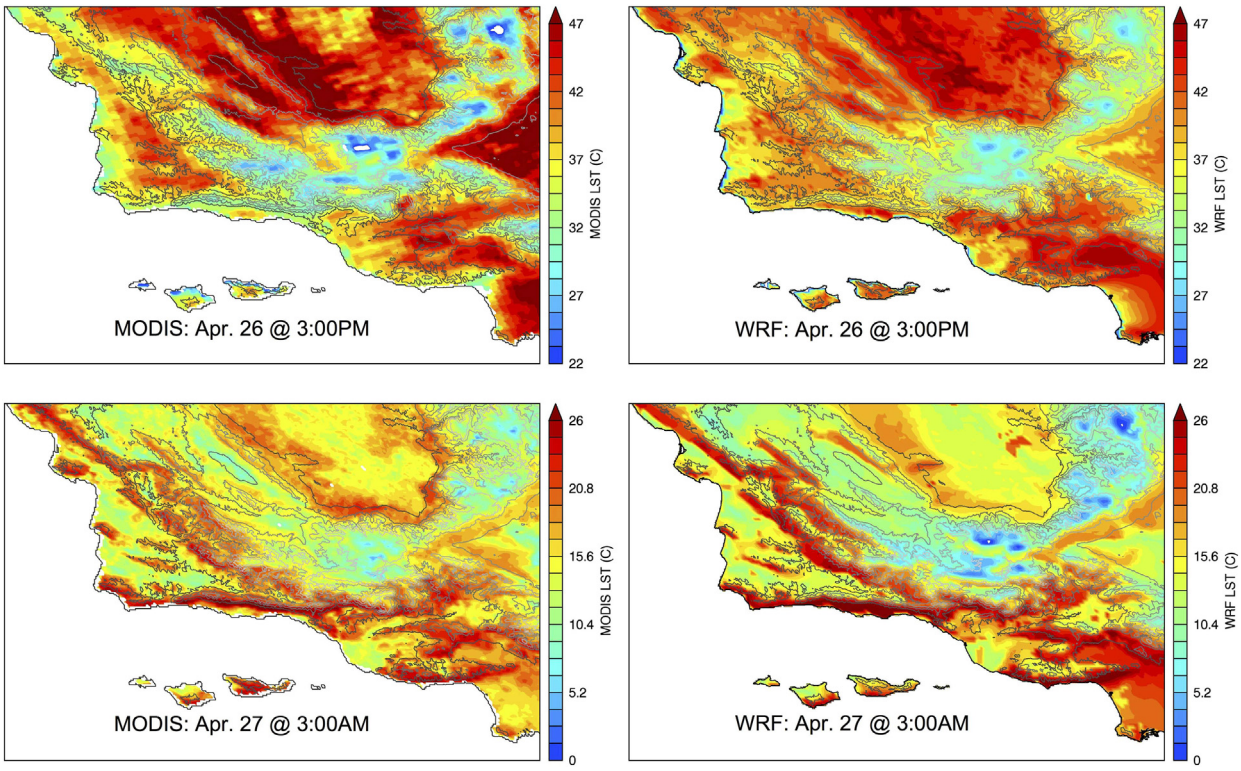

Fig. 6. MODIS land surface temperature estimates at 3:00 PM on April 26th, 2004 (top left) and at 3:00 AM PST on April 27th (bottom left). WRF-simulated skin temperature estimates for the corresponding times (right column).

limitation to comprehensively evaluating the skill of WRF in simulating these events. Analyses of the evolution of the studied sundowner events in the following section should be interpreted with caution given uncertainties in the model. Although absolute values may disagree between model and observation, the temporal evolution of the event is apparently well represented, and thus WRF can be used with confidence to evaluate sundowner events based on tendencies in each relevant variable.

6. Discussion: sundowner dynamics — case study

6.1. Surface temperature and relative humidity

This section discusses the dynamical evolution of the peak sundowner event during the simulated period, as well as the collective conditions that led to events on individual nights throughout the simulation, in order to identify mechanisms that factored into their development.

Fig. 7 shows 2 m temperature and 10 m wind during the peak of the strongest sundowner event within the simulation, occurring on April 27th at 3:00 AM (local time), and the composite 2 m temperature and 10 m wind for the peak of 5 individual sundowner events on different nights within the simulation. In contrast to typical nighttime temperatures, pronounced heating is observed on the southern slope of the Santa Ynez Mountains in the early morning of April 27th, as well as in the composites of all sundowner events in the study period. WRF-composite relative humidity for the five sundowner events is also presented in Fig. 7. Considerable decreases in relative humidity are observed co-located with downslope winds and temperature increases on the southern side of the Santa Ynez Mountains.

The conditions observed in Fig. 7 exemplify the characteristics of "sundowner" winds, which are marked by adiabatic warming of downslope winds. It is notable that the winds in the composites generally do not extend beyond the coastline, where the marine layer dominates. However, in observing the temporal evolution of individual events, it is apparent that winds do extend across the Santa Barbara Channel periodically and that the most intense region of offshore winds propagates from west to east at onset and east to west at demise, which corresponds to the evolution of pressure gradients between SB and Santa Maria and SB and Bakersfield over the course of the night. This is also difficult to validate given the limited sampling of available observations and notable issues with WRF's simulation of the coastal environment (Huang et al., 2013, and previous section).

6.2. Spatial patterns of pressure

The development of the sundowner event is best understood through the spatial evolution of mesoscale pressure gradients over the course of the day, which led to the observed low-level winds. Here, we also discuss the effectiveness of one particular tool the NWS/LOX currently uses to help forecast sundowner development, which is based on a linear scaling of observed wind speed at Santa Barbara with pressure differences between Santa Barbara (Station #2 in Fig. 1) and Bakersfield (Station #12) and Santa Barbara and Santa Maria (Station #8) (Sukup, 2013).

Fig. 8 demonstrates the temporal evolution of sea-level pressure over the domain before and during the sundowner event in the early morning hours of April 27th. The complexity of the mesoscale circulation around this event is attributable to orographic effects and land-sea contrast, which modify pressure gradients through heating differences and dynamical influences over the course of the day. The diurnal cycle of pressure is largest in inland mountain regions, where low sea-level pressure is observed in the afternoon on account of strong diabatic heating, and transitions quickly to high pressure after sunset with increasing local stability driven by radiative cooling. In the afternoon, pressure offshore is relatively higher than inland and onshore flow develops. This occurs asymmetrically as the coastal pressure gradient is modified by regional topography. Notably, the SB Channel maintains lower pressure than over outer waters west of Pt. Conception throughout the study period. This may occur because of slightly warmer water in the channel and the development of a lee vortex as northwest

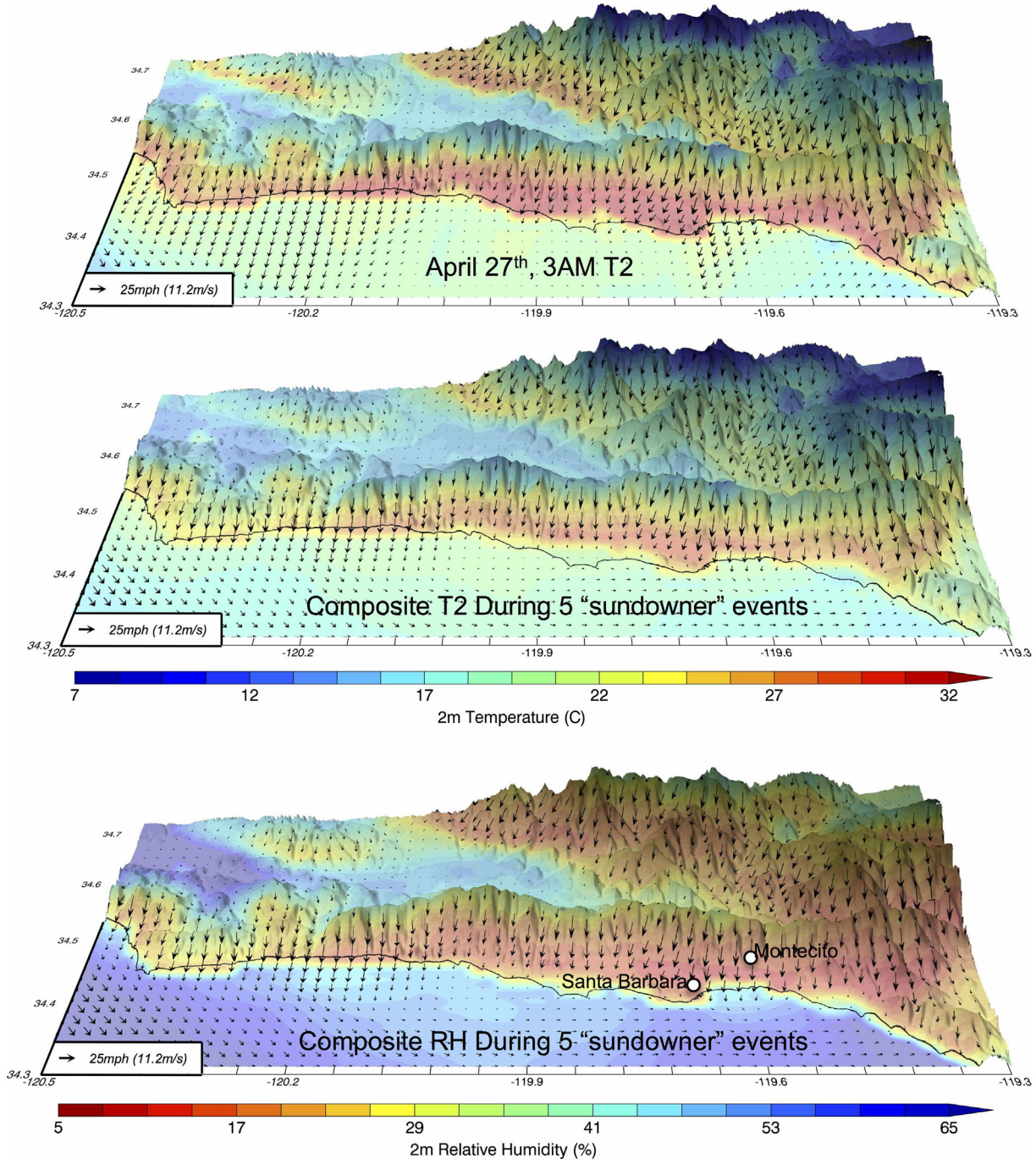

Fig. 7. 2 m temperature and 10 m winds on April 27th at 3:00 AM PST (top). Composite 2 m temperature and 10 m wind during the peak period of 5 sundowner events in the 2004 case study (middle). Composite 2 m relative humidity and 10 m wind during the peak period of 5 sundowner events in the 2004 case study (bottom). The location of the Montecito Hills station, above downtown Santa Barbara is labeled for reference.

winds pass Pt. Conception (Fig. 1 for reference). A strong pressure gradient is observed over the SB area in all frames of Fig. 8. The gradient exhibits a very rapid transition from onshore to offshore at sunset that is in agreement with the typical rapid development of offshore wind in the evenings (Dorman and Winant, 2000). As the evening progresses, the mesoscale low in the Santa Barbara channel is intensified by adiabatic heating from offshore downslope winds. Also, the diurnal evolution of an east-west pressure gradient across the valley north of the Santa Ynez Mountains contributes to spatial and temporal variability in the strength of winds along the Santa Barbara coast.

With respect to the NWS forecasting methodology of evaluating pressure differences between Santa Barbara and Bakersfield and Santa Barbara and Santa Maria to forecast wind speed and direction, it appears that though these metrics are useful in establishing whether winds will develop, much of the spatial complexity of the pressure gradients and their evolution are ignored by this simple forecasting approach. The analysis of Fig. 8 identifies a complex pressure gradient that is constantly evolving, spatially and temporally, as a result of a wide variety of mechanisms, such as the breakup of the marine layer, the development of a lee vortex around Point Conception and mesoscale perturbations in pressure associated with heating and cooling effects in the mountains, which are unaccounted for in station analysis. Given WRF's skill in simulating observed sea-level pressure (Table-2), considerable information on the spatial pattern of pressure tendencies can be garnered from WRF

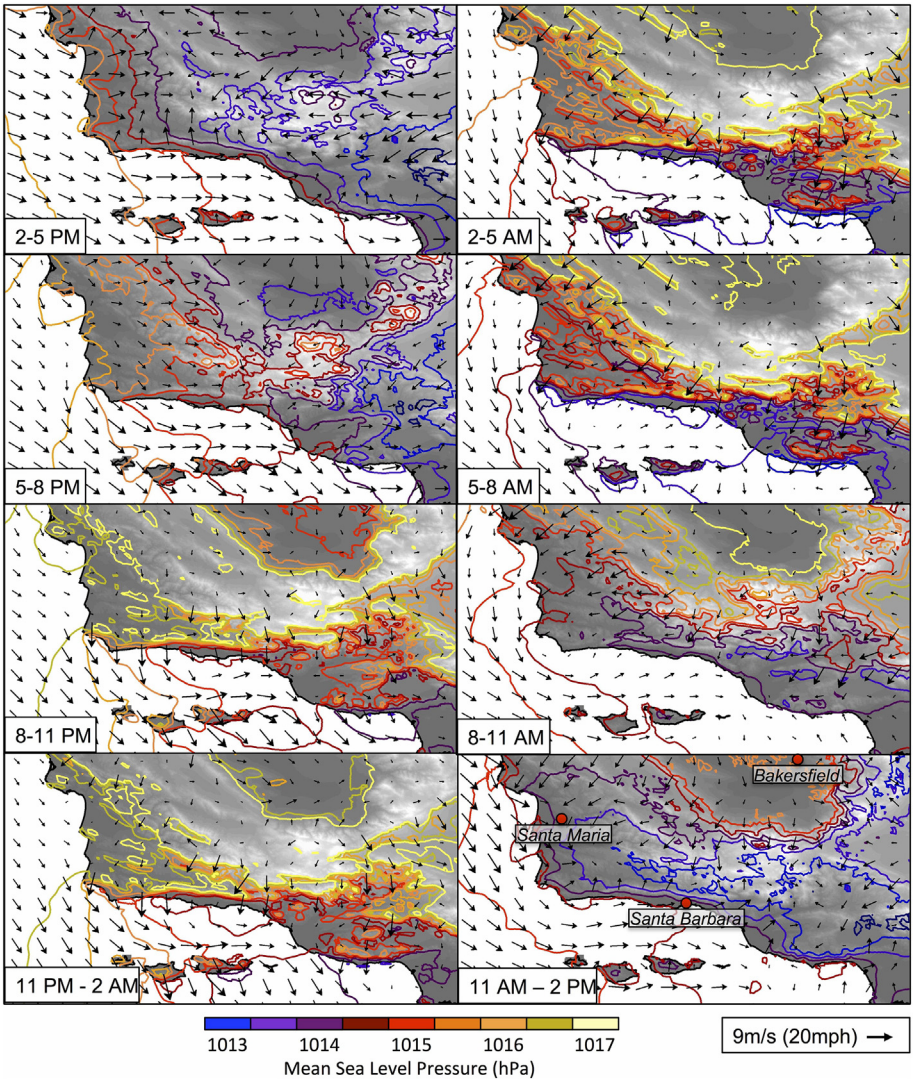

Fig. 8. Mean sea level pressure (color contours), topography (gray shade) and average 10 m wind for 3-hour time steps from 2 PM on April 26th (top left) to 2 PM on April 27th, 2004 (bottom right; local time). (For interpretation of the references to color in this figure legend, the reader is referred to the web version of this article.)

to aid in forecasting of northerly surface winds and better understanding spatial and temporal variability in sundowner winds.

6.3. Vertical profile of sundowner winds

The vertical structure of meridional wind for a north-south transect at the longitude of the Montecito station during the peak of sundowner activity on April 27th is shown in Fig. 9. At upper levels, large-scale northwesterly flow prevails, and strong northerly winds are observed between 10 and 15 km. Surface high pressure over the Great Basin generates southeasterly flow through the daytime hours up to 5 km, but during the night the lowest levels turn offshore (Fig. 8). Radiative cooling inland appears to generate northerly flow that extends from the Sierra Nevada (north of the inner domain extent) into the Southern California Bight. The directional shear in the vertical profile was also observed in the Vandenberg sounding at 5 AM local time (not shown). Over the coastal ranges northerly flow generates a lee gravity wave within the strongly stratified coastal environment at night (Fig. 9).

Generally, the primary mechanisms that induce downslope windstorms within an environment that supports lee gravity waves include an inversion above the mountaintop and either velocity or directional shear of the cross-barrier wind (Durran, 1990). Trapped lee waves, confined to the lower troposphere on the lee side of the mountains, result from an increase in wind speed, a decrease in stability, or an increase in the curvature of the wind speed profile. These atmospheric conditions inhibit the buoyancy-driven oscillation of a gravity wave and thus its energy is reflected back to the surface.

A metric that is frequently used in forecasting trapped lee waves is the scorer parameter, defined by Scorer (1949) as:

$$l^2 = \frac{N^2}{U^2} - \frac{1}{U}\frac{\partial^2 U}{\partial z^2} \quad (1)$$

where $N(z)$ is the Brunt Vaisala frequency, and $U(z)$ is the mean cross-barrier horizontal wind speed, and z is the vertical coordinate. Scorer (1949) demonstrated that trapped lee waves occur only when l^2 decreases with height, which can result from an increase in cross-mountain wind speed, a decrease in stability, or an increase in the curvature of the wind speed profile. The l^2 metric has been used to study mountain waves in experiments (e.g. Grubisic and Billings, 2007 for the Owens Valley, CA) and is applied in operational forecasting for certain regions (e.g. Shutts, 1997). Ryan (1996) and Sukup (2013) noted the importance of an inversion layer above the mountaintop for reflecting gravity wave energy toward the surface in sundowner cases, but did not discuss the role of the wind profile, thus only partially addressing lee-wave trapping.

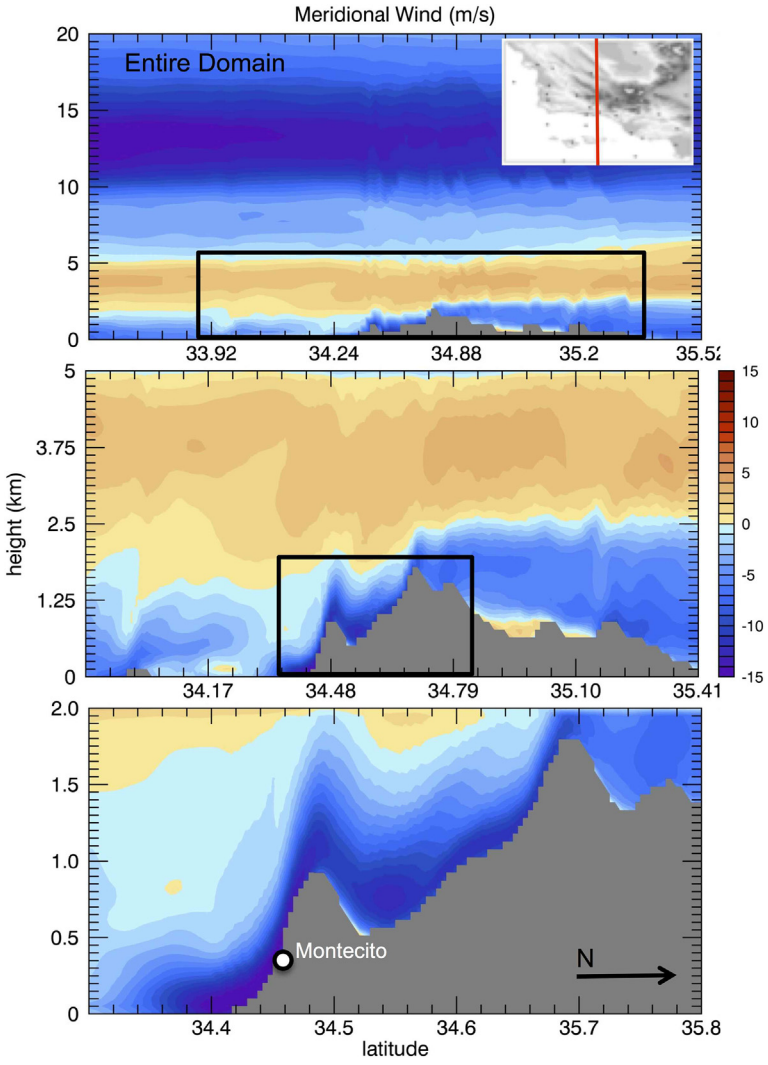

Fig. 9. North-south transect of meridional wind speed for all model levels (top) at the longitude of the Montecito Hills station (indicated by red line across the topography map in upper right corner). The black boxes indicate regions of interest that are focused on in the panel below. Gray shade in each panel indicates topography. (For interpretation of the references to color in this figure legend, the reader is referred to the web version of this article.)

Additionally, downslope winds may occur in the presence of a mean-state critical layer, which forms due to directional shear in the cross-barrier flow, or a self-induced critical layer, which forms due to turbulence from gravity wave breaking. A critical layer impedes the vertical propagation of wave energy at certain wavelengths, thus deflecting considerable energy into near-surface wind speed on the lee slope (Durran, 2003). No previous studies have investigated the role of directional shear or wave breaking in developing a critical layer and contributing to downslope wind intensification in sundowner events. The Richardson Number, defined as:

$$Ri = \frac{N^2}{(\partial U/\partial z)^2} \tag{2}$$

is used here to investigate whether self-induced critical layers contributed to sundowner development during the study period. A Richardson Number of <0.25 is indicative of turbulent flow that may reflect mountain wave energy, consistent with a critical layer (Durran, 1990).

Conditions that support trapped lee waves, identified by rapidly decreasing l^2 (Eq. (1)), were not found in the 2004 case study. Rather, the Scorer Parameter (l^2) increased dramatically in the region of cross-barrier flow reversal, where the mean cross barrier wind approaches zero (grayshade in Fig. 10, middle panel), creating a mean-state critical layer. Additionally, below the region of cross-barrier flow reversal at ~2 km elevation, the Richardson Number (Eq. (2)) was generally <1 and approached 0.25 in select locations, indicating the potential for turbulence below the mean-state critical layer. These conditions may support a self-induced critical layer that potentially contributed to the acceleration of downslope winds in the case study, although the primary influence appears to be the mean-state critical layer. From Fig. 10, it can be seen that mountain waves induced by northerly wind over topography do not propagate beyond the mean-state critical layer at the level of cross-barrier flow reversal, where wave energy is reflected toward the surface according to its wavelength (Durran, 2003; Zhang et al., 2014). The establishment of a mean-state critical layer was observed for all nights with sundowner events in the study period. The Brunt Vaisala frequency and curvature terms of the Scorer Parameter (Eq. (1)) indicated that trapped lee waves were not a primary influence in this case.

The vertical profiles shown in the bottom panels (Fig. 10) elucidate the relationship between winds, the Scorer Parameter and Richardson Number, and their relationship with the propagation of gravity wave energy and downslope winds. In the sundowner case (left panel) the reversal in cross-barrier wind at 1.6 km above the Montecito station corresponds to a rapid 'jump' in the Scorer Parameter. Below the mean-state critical layer at 1.6 km, several model levels exhibited Richardson

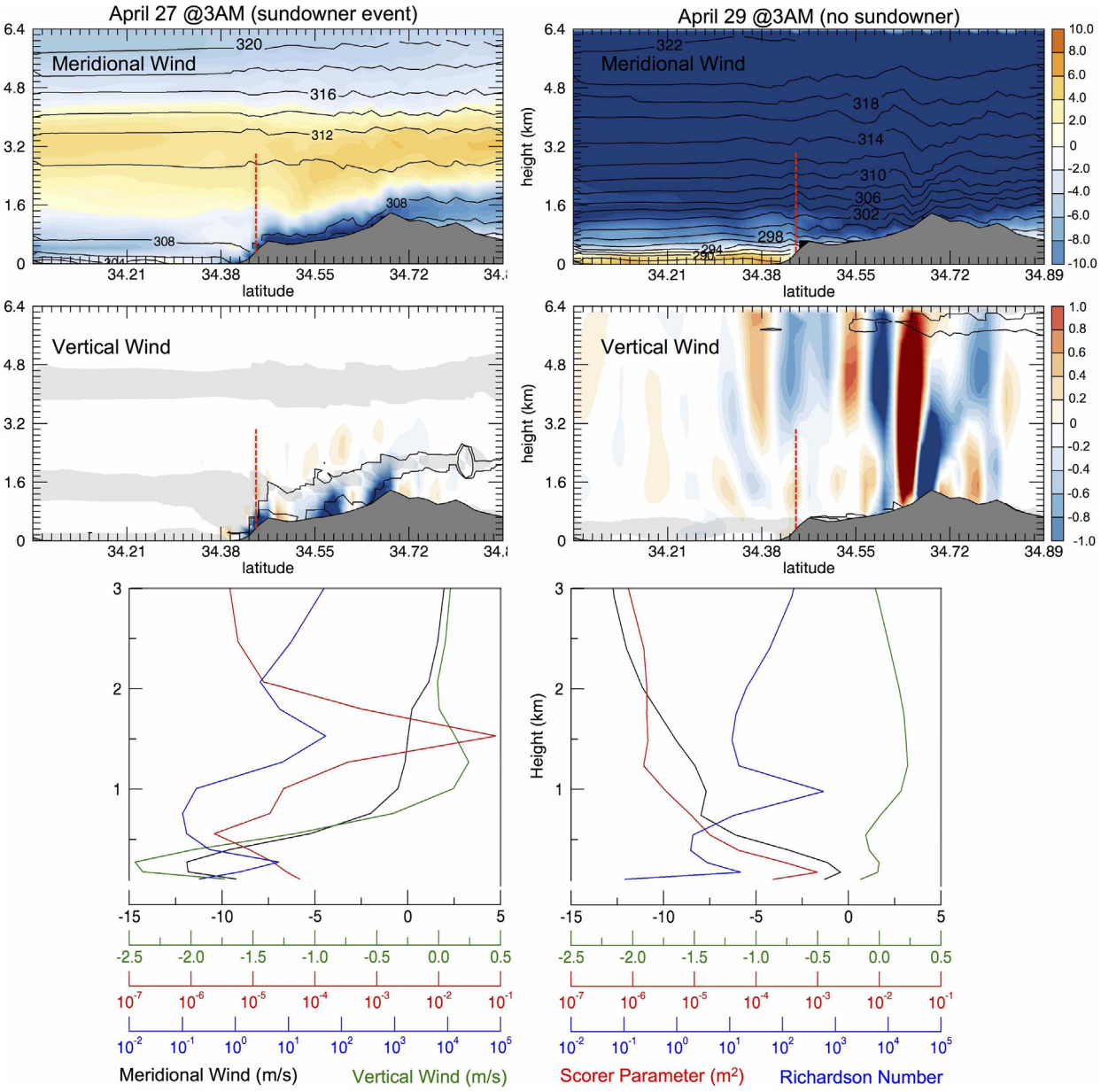

Fig. 10. North-South transects of meridional wind (color) and theta (contours) (top panels) and vertical velocity (middle) at the longitude of the Montecito Hills station (topography is masked in grayshade) for April 27th at 3:00 AM (left column) and April 29th at 3:00 AM PST (right column). The black contour in the vertical wind profiles indicate Richardson Number < 1, and light gray shading indicates 'undefined' values of the Scorer Parameter, resulting from a near-zero *U* component in Eq. (1) at the level of cross-barrier wind reversal. The red dashed lines in the top and middle panels indicate the location of the vertical profile shown in the bottom panel. (For interpretation of the references to color in this figure legend, the reader is referred to the web version of this article.)

Numbers approaching 0.25, indicating the possibility of turbulence and a self-induced critical layer that further accelerated downslope wind by constraining wave energy to a shallow region above the mountain height. Downward vertical velocity near the surface was near 2.5 m/s and northerly wind exceeded 12 m/s (~27 mph).

Fig. 10 (right panel) displays a case without sundowner activity during the study period that experienced northerly wind velocities in excess of those observed during the sundowner event, and a vertical gradient of potential temperature that indicates a considerably more stable atmosphere. In this case, occurring on April 29th, winds did not reverse with height, and the Scorer Parameter decreased uniformly with increasing wind speed aloft. A mean-state critical layer was not observed near the mountaintop, and the Richardson Number at all levels was larger than the range indicative of a self-induced critical layer. Consequently, gravity waves formed by northerly wind across the mountain barrier propagated vertically rather than reaching the surface in the lee of topography. In this case it is possible that the marine layer, identified by stable southerly flow below the mountain height, also factored into the absence of downslope winds.

The identification of critical layers above the mountain height and/or conditions that support trapped lee waves, using the Richardson Number and Scorer Parameter, are potentially useful for improving forecasts of sundowner wind events. The 2004 case study demonstrates the influence of a mean-state critical layer above the mountaintop in reflecting energy toward the surface and intensifying downslope winds, with the potential support of light turbulence. Although trapped lee waves were not influential in this event, previous research infers that the Scorer Parameter may also be useful in other events where either velocity shear or mountaintop inversions contribute to downslope wind intensification. It is necessary to investigate additional sundowner events as

well as events with strong northerly winds aloft that did not generate downslope winds to more generally understand the mesoscale dynamics that drive sundowner evolution.

7. Hindcasts of major fires associated with strong downslope winds

WRF simulations with 2 km resolution were performed for 5-day periods encompassing the outbreak dates of the Painted Cave Fire (June 27th, 1990) and the Jesusita Fire (May 5, 2009), to evaluate the prevailing conditions with respect to the mechanisms that produced the 2004 event. These two fires were fueled by intense sundowner winds on successive nights after each fire's ignition. The Painted Cave Fire, noted as the most destructive in SB history, burned 20.23 km^2 (5000 acres), destroyed 427 buildings, killed 1 civilian and caused more than $270 million in damages according to the California Department of Forestry and Fire Protection (CalFire). The Jesusita fire burned 35.27 km^2 (8733 acres), destroyed 80 homes and forced the evacuation of an estimated 15,000 people, with an estimated economic cost of $20 million. In both cases, the mesoscale dynamics that generated the sundowner winds in the 2004 case study are prevalent, despite considerable differences in the synoptic weather patterns. These results identify important commonalities among events generated by different large-scale conditions, thus giving confidence to the utility of understanding the general evolution sundowner winds through a small sample of events, including some notable dates in SB fire history.

Fig. 11 shows 2 m relative humidity and 10 m winds at the time of ignition for the Painted Cave Fire, and during the peak sundowner winds following the ignition of the Jesusita Fire. The Painted Cave fire occurred during extreme sundowner conditions, with sustained surface winds in excess of 15 m/s (~34 mph) over the foothills, relative humidity values of <10% and temperatures above 38 °C (100 °F). Contrastingly, the strong northerly adiabatically-warmed winds (maximum wind speed = 14 m/s or 31.3 mph) during the Jesusita event were not as dry (min RH in foothills = 13%) and temperatures were considerably cooler (max T2 m in foothills = 31.6 °C or 87 °F).

In each of the studied cases, the common ingredient was the presence of a north-south mean sea level pressure gradient across the Santa Ynez Mountains, which produced northerly winds perpendicular to the mountain barrier, as Blier (1998) noted was necessary. However, the large-scale conditions that generated the pressure gradient were unique to each event studied. Fig. 12 shows mean sea level pressure and 500-hPa geopotential height daily composites on the date of peak sundowner activity from the 2004 event and both investigated fires. Notably, the Painted Cave and Jesusita fire events were not associated with a blocking ridge over the Western US, as was observed in the 2004 event. Contrastingly, high pressure was observed in the lower troposphere off of the California coast and low pressure was observed over the Great Basin, thus creating a strong zonal pressure gradient over California and northerly geostrophic winds in the lower atmosphere (not shown). Additionally, the two fire events featured strong meridional pressure gradients aloft, which created intense west/southwesterly flow through the middle and upper troposphere.

Despite differences in the synoptic conditions surrounding the Painted Cave Fire, the Jesusita Fire, and the 2004 case study, all three periods of sundowner activity were generated by northerly wind over the Santa Ynez Mountains. Fig. 13 shows meridional and vertical wind profiles along the Montecito Hills longitude transect during the peak of northerly surface wind in the Montecito Hills location in the 2004 case study, at 3:00 AM on the 27th, as well as at 3:00 AM on the night following the ignition of each fire. Northerly meridional flow exceeding 10 ms^{-1} was observed near the surface in the lee of topography, and was responsible for generating a mountain wave with vertical velocities in excess of 2 ms^{-1} in all cases. From the 2004 composite, it is apparent that the weakening and reversal of meridional wind between 2 and

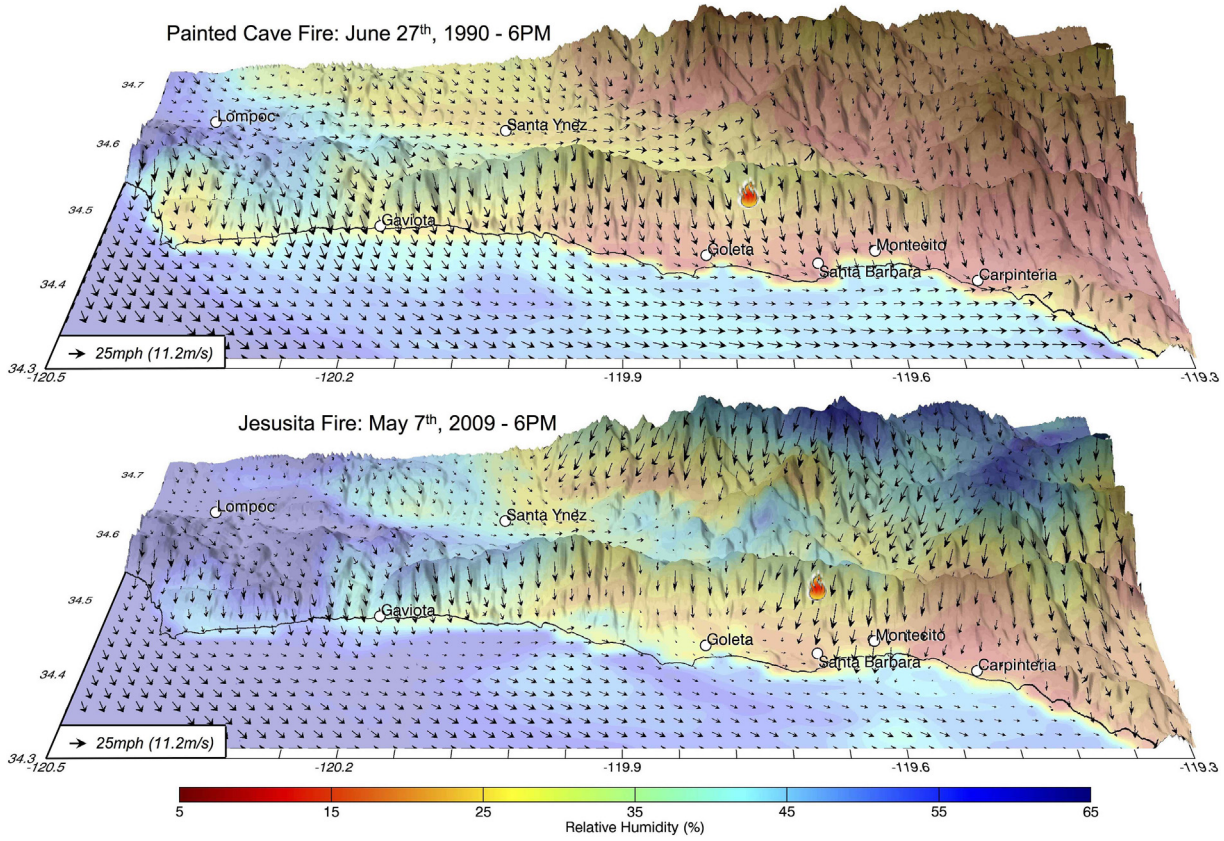

Fig. 11. 2 m relative humidity and 10 m wind speed at 6:00 PM PST on June 27th, 1990 (top). 2 m relative humidity and 10 m wind speed at 6:00 PM PST on May 5th, 2009 (bottom). Cities are labeled with white dots and the fire symbol indicates the point of ignition for each period's fire.

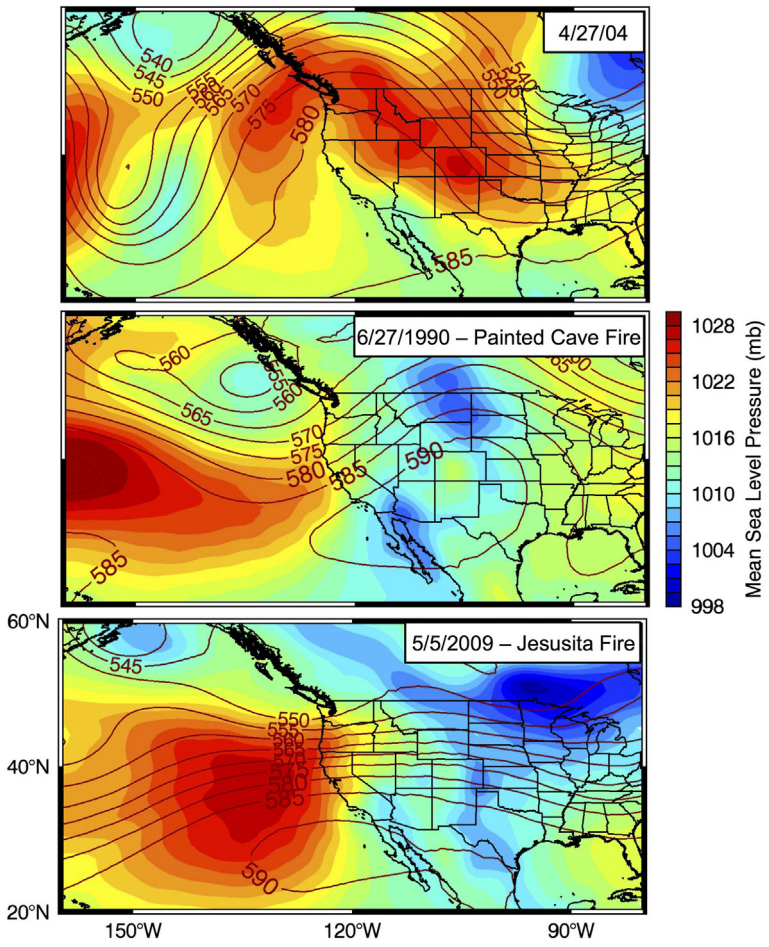

Fig. 12. CFSR daily averaged mean sea level pressure (color) and 500-hPa geopotential height (contour) for the peak sundowner periods in the 2004 case study (top), Painted Cave Fire (middle) and Jesusita Fire (bottom). (For interpretation of the references to color in this figure legend, the reader is referred to the web version of this article.)

5 km elevation (as evidenced by Fig. 10) resulted in a mean-state critical layer that trapped gravity wave energy near the mountaintop over the course of the event. In the Painted Cave event, a flow reversal and mean-state critical layer were also observed roughly 3 km above ground level, and a self-induced critical layer is apparent in the region of wave activity near the surface ($Ri < 0.25$). During the Jesusita event, which also featured west/southwesterly flow aloft related to an upper-level trough, northerly flow was observed up to 8 km and thus, without distinct atmospheric layers, gravity waves propagated vertically to a greater extent. In the Jesusita case, northerly cross-barrier winds near the surface exceeded 20 ms^{-1}, which led to considerably larger amplitude gravity waves and wave breaking. The upstream-tilting isentropes and reversed/turbulent flow above the mountaintop in this case are indicative of gravity wave breaking and a self-induced critical layer ($Ri < 0.25$; Durran, 1990) that generated downslope acceleration over Santa Barbara, in the absence of a mean-state critical layer.

8. Conclusions

Frequent gusty downslope winds, accompanied by rapid warming and decreased relative humidity, commonly termed “sundowners” are among the most significant weather events affecting Southern California coastal areas in the vicinity of Santa Barbara (SB). Sundowners greatly increase fire, aviation and maritime navigation hazards and are thus a priority for regional forecasting. This work aims to both evaluate the efficacy of the WRF model in simulating sundowner events, and to improve our understanding of the dynamics that are responsible for the evolution of these events. Here, we perform the first systematic study to evaluate the skill of WRF in simulating sundowner events, focusing on a case study period in late April through early May 2004. Multiple WRF configurations were evaluated against available observational data.

Accurate prediction of the onset, duration and demise of sundowners, in addition to their spatial and temporal heterogeneity across the SB foothills are crucial to fire decision support for the U.S. Forest Service and the SB County Fire Department. Currently, WRF (at 2 km resolution, and with the configuration tested in this study) complements the NWS forecast at regional-to-local scales.

Overall, this study indicated that WRF properly simulated the evolution of near-surface temperature, pressure and wind direction over the entire domain during the studied event. However, WRF underestimated wind speed, and demonstrated significant issues in representing the marine layer, which altered the influence of downslope winds over the SB coastal plain. Furthermore, available station data for validation is relatively sparse, and there is no effective way to validate WRF vertical profiles from the single radiosonde in the study domain. Sensitivity tests confirmed that the parameterization scheme currently in operation at the NWS is optimal (among those tested), although, differences among WRF configurations were small compared to differences between observations and simulation.

WRF output from the NWS configuration with 2 km horizontal resolutions were used to investigate dynamical mechanisms explaining the evolution of sundowner events during the case-study. In accordance with the necessary conditions for sundowner winds identified by Blier (1998), the April 2004 events exhibited strong northerly winds across the Santa Ynez Mountains that peaked in intensity overnight. These

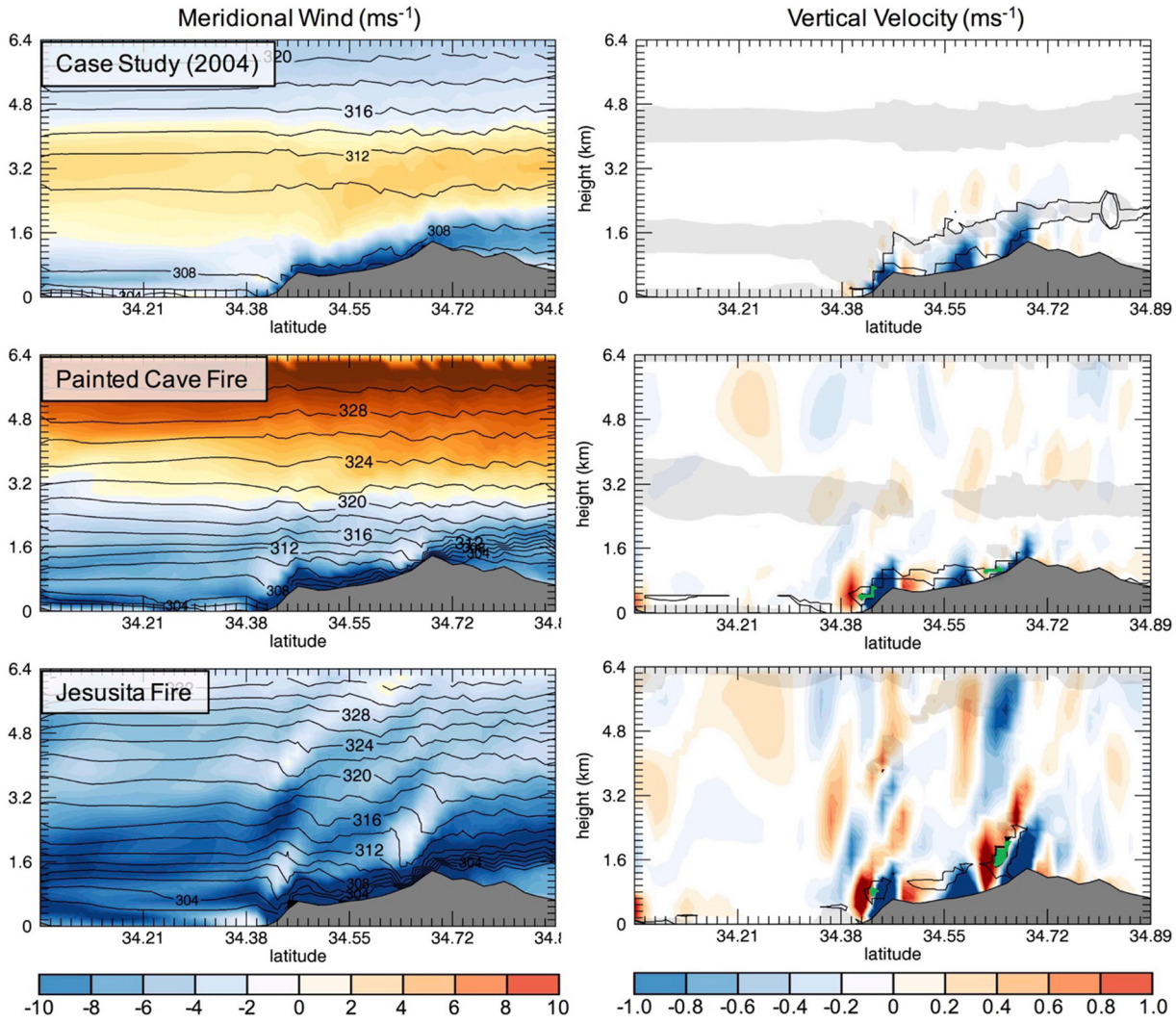

Fig. 13. North-South transects of meridional wind (left column) and vertical velocity (right column) at the longitude of the Montecito Hills station for peak sundowner periods in the 2004 case study – April 27th, 2004 at 3 AM local time (top row), the Painted Cave Fire – June 28th, 1990 at 3:00 AM (middle row) and the Jesusita Fire May 6th, 2009 at 3:00 AM (bottom row). Topography is shaded dark gray. Black contours in the left column indicate theta at 2° increments. The black contour in the right column indicates $Ri < 1.0$, and green shading indicates $Ri < 0.25$. Light gray shading indicates a region of 'undefined' Scorer Parameter, resulting from a near-zero U component in Eq. (1) at the level of cross-barrier wind reversal. (For interpretation of the references to color in this figure legend, the reader is referred to the web version of this article.)

northerly cross barrier winds in the prevailing strongly-stratified nighttime environment generated gravity waves in the lee of the coastal range that accelerated winds on the downslope side of the mountains. Notably, this study identified the presence of a critical layer (Durran, 1990) that aided in the enhancement of downslope winds over the SB foothills and coastal plain. A mean-state critical layer, attributable to wind backing and reversal with height in the lower troposphere above the mountaintop in this case, reflected gravity wave energy back to the surface (Durran, 2003). Additional studies are required to fully investigate the utility in identifying both mean-state and self-induced critical layers for sundowner forecasting purposes.

Finally, we performed hindcasts of two major fire events in Santa Barbara: the Painted Cave Fire and the Jesusita Fire. Both events were driven by sundowner winds, and our goal was to identify commonalities among these and the 2004 case study. Although northerly winds and subsequent gravity waves during the two fire events originated from large-scale forcing that was dissimilar to that observed in the 2004 case study, the basic mesoscale conditions responsible for the 2004 sundowner event were present in both the Painted Cave and Jesusita events. Despite broad commonalities, the spatial structure of the sundowner winds, their orientation, intensity and extent over the coastal plain varied greatly in each case at scales important for fire decision support. Assuming accurate representation of observations, the resolution of these mesoscale complexities on a case by case basis may greatly aid in the forecasting of local winds, which are crucial to supporting fire management agencies' resource allocation. Furthermore, evaluation of the vertical structure of these events aids in our general understanding of how sundowners evolve. In the investigated cases, the vertical profile of wind and stability were important in determining why downslope winds were intensified relative to cases when northerly cross-barrier winds did not intensify into near-surface sundowners.

Ultimately, diagnostics such as the Richardson Number and Scorer Parameter may be useful for forecasting conditions that contribute to sundowner wind development, including cross-barrier flow reversal, mountaintop inversions, and self-induced critical layers. However, it is clear that a considerable amount of work needs to be done to understand model deficiencies as well as the evolution of sundowner events to improve their prediction. This manuscript only begins to address these issues, though it represents an important step for an understudied problem of considerable consequence to the Santa Barbara region.

Acknowledgements

This study was made possible in part due to the data made available by the governmental agencies, commercial firms, and educational institutions participating in MesoWest. The CFSR data used in this research were developed by NOAA's National Centers for Environmental Prediction (NCEP) and provided by NCAR. Atmospheric soundings for the Vandenberg station were procured from the University of Wyoming, Department of Atmospheric Science. http://weather.uwyo.edu/upperair/sounding.html. We also thank two anonymous reviewers for their detailed and astute comments, which were extremely helpful.

References

Beljaars, A.C.M., et al., 1994. The parameterization of surface fluxes in large-scale models under free convection. Quart. J. Roy. Meteor. Soc. 121, 255–270.
Blier, W., 1998. The sundowner winds of Santa Barbara, California. Wea. Forecasting 13, 702–716.
Brinkman, W.A.R., 1971. What is a foehn? Weather 26, 230–240.
Caldwell, P., Chin, H.N.S., Bader, D.C., Bala, G., 2009. Evaluation of a WRF dynamical downscaling simulation over California. Clim. Chang. 95, 499–521.
Casey, K.S., Brandon, T.B., Cornillon, P., Evans, R., 2010. The past, present and future of the AVHRR pathfinder SST program. In: Barale, V., Gower, J.F.R., Alberotanza, L. (Eds.), Oceanography from Space: Revisited. Springer http://dx.doi.org/10.1007/978-90-481-8681-5_16.
Chin, H.N.S., Caldwell, P.M., Bader, D.C., 2010. Preliminary study of California wintertime model wet bias. Mon. Weather Rev. 138, 3556–3571.
Chow, F.K., De Wekker, S.F.J., Snyder, B. (Eds.), 2012. Mountain Weather Research and Forecasting: Recent Progress and Current Challenges. Springer, Berlin.
Dorman, C.E., Winant, C.D., 2000. The structure and variability of the marine atmosphere around the Santa Barbara Channel. Mon. Weather Rev. 128 (1), 261–282.
Doyle, J.D., Shapiro, M.A., 1999. A multi-scale simulation of an extreme downslope windstorm over complex topography. Meteorog. Atmos. Phys. 74, 83–101.
Doyle, J.D., et al., 2011. An intercomparison of T-REX mountain-wave simulations and implications for mesoscale predictability. Mon. Weather Rev. 139, 2811–2831.
Dudhia, J., 1989. Numerical study of convection observed during the winter monsoon experiment using a mesoscale two-dimensional model. J. Atmos. Sci. 46, 3077–3107.
Dulière, V., Zhang, Y., Salathé Jr., E.P., 2011. Extreme precipitation and temperature over the US Pacific northwest: a comparison between observations, reanalysis data, and regional models. J. Clim. 24 (7), 1950–1964.
Durran, D.R., 1990. Mountain waves and downslope winds. Meteorol. Monogr. 23, 60–83.
Durran, D.R., 2003. Lee waves and mountain waves. Encyclopedia of Atmospheric Sciences. 1161–1169.
Grubisic, V., Billings, B., 2007. The intense lee-wave rotor event of sierra rotors IOP8. J. Atmos. Sci. 64, 4178–4201.
Grubisic, V., Billings, B., 2008. Summary of the sierra rotors project wave and rotor events. Atmos. Sci. Lett. 9, 176–181.
Holton, J.R., 2004. An Introduction to Dynamic Meteorology. Elsevier Academic, Burlington, MA.
Hong, S.Y., Dudhia, J., Chen, S.H., 2004. A revised approach to ice microphysical processes for the bulk parameterization of clouds and precipitation. Mon. Weather Rev. 132, 103–120.
Hong, S.Y., Noh, Y., Dudhia, J., 2006. A new vertical diffusion package with an explicit treatment of entrainment processes. Mon. Weather Rev. 134, 2318–2341.
Huang, H.Y., Hall, A., Teixeira, J., 2013. Evaluation of the WRF PBL parameterizations for marine boundary layer clouds: cumulus and stratocumulus. Mon. Weather Rev. 141, 2265–2271.
Iacono, M.J., Delamere, J.S., Mlawer, E.J., Shephard, M.W., Clough, S.A., Collins, W.D., 2008. Radiative forcing by long–lived greenhouse gases: calculations with the AER radiative transfer models. J. Geophys. Res. 113, D13103.
Jiang, Q., Doyle, J.D., 2008. Diurnal variation of downslope winds in Owens Valley during the sierra rotor experiment. Mon. Weather Rev. 136, 3760–3780.
Kain, John S., 2004. The Kain–Fritsch convective parameterization: an update. J. Appl. Meteorol. 43, 170–181.
Klemp, J.B., Lilly, D.K., 1975. The dynamics of wave induced downslope winds. J. Atmos. Sci. 32, 320–339.
Lawson, J., Horel, J., 2015. Analysis of the 1 December 2011 Wasatch downslope windstorm. Wea. Forecasting 30, 115–135.
Mlawer, E.J., Taubman, S.J., Brown, P.D., Iacono, M.J., Clough, S.A., 1997. Radiative transfer for inhomogeneous atmospheres: RRTM, a validated correlated-k model for the longwave. J. Geophys. Res. 102, 16663–16682.
Morrison, H., Thompson, G., Tatarskii, V., 2009. Impact of cloud microphysics on the development of trailing Stratiform precipitation in a simulated squall line: comparison of one- and two-moment schemes. Mon. Weather Rev. 137, 991–1007.
Nakanishi, M., Niino, H., 2009. Development of an improved turbulence closure model for the atmospheric boundary layer. J. Meteor. Soc. Japan 87, 895–912.
Ryan, G., 1996. Downslope Winds of Santa Barbara County, California. Western Region Technical Memorandum NWS WR-240. National Weather Service Western Region, Oxnard, California.
Saha, S., et al., 2010. The NCEP climate forecast system reanalysis. Bull. Am. Meteorol. Soc. http://dx.doi.org/10.1175/2010BAMS3001.1 (1015-057).
Scarino, A.J., Obland, M.D., Fast, J.D., Burton, S.P., Ferrare, R.A., Hostetler, C.A., Berg, L.K., Lefer, B., Haman, C., Hair, J.W., Rogers, R.R., Butler, C., Cook, A.L., Harper, D.B., 2014. Comparison of mixed layer heights from airborne high spectral resolution lidar, ground-based measurements, and the WRF-Chem model during CalNex and CARES. Atmos. Chem. Phys. 14, 5547–5560.
Scorer, R.S., 1949. Theory of waves in the lee of mountains. Q. J. R. Meteorol. Soc. 75, 41–56.
Shutts, G., 1997. Operational lee wave forecasting. Meteorol. Appl. 4, 23–35.
Skamarock, W.C., Klemp, J.B., Dudhia, J., Gill, D.O., Barker, D.M., Duda, M.G., Huang, X.Y., Wang, W., Powers, J.G., 2008. A Description of the Advanced Research WRF Version 3. NCAR Technical Note NCAR/TN-475+STR. (125 pp.). NCAR, Boulder, CO.
Smith, R.B., 1979. The influence of mountains on the atmosphere. Adv. Geophys. Vol. 21, 87–230 (Academic Press).
Smith, R.B., 1985. On severe downslope winds. J. Atmos. Sci. 42, 269–297.
Smith, B.L., Yuter, S.E., Neiman, P.J., Kingsmill, D.E., 2010. Water vapor fluxes and orographic precipitation over northern California associated with a landfalling atmospheric river. Mon. Weather Rev. 138 (1), 74–100.
Sukup, S., 2013. Extreme Northeasterly Wind Events in the Hills Above Montecito, California. Western Region Technical Attachment NWS WR-1302. National Weather Service Western Region, Salt Lake City, UT.
Tewari, M., Chen, F., Wang, W., Dudhia, J., LeMone, M.A., Mitchell, K., Ek, M., Gayno, G., Wegiel, J., Cuenca, R.H., 2004. Implementation and verification of the unified NOAH land surface model in the WRF model. 20th conference on weather analysis and forecasting/16th conference on numerical weather prediction 11–15.
Walton, D.B., Sun, F., Hall, A., Capps, S., 2015. A hybrid dynamical–statistical downscaling technique. Part I: Development and validation of the technique. J. Clim. 28, 4597–4617.
Wan, Z., 1999. MODIS land-surface temperature algorithm basis document (LST ATBD) (version 3.3).
Zhang, P., Lahourai, B., Imhoff, M., Wolfe, R., Thome, K., 2014. Comparison of MODIS land surface temperature and air temperature over the continental USA meteorological stations. Can. J. Remote. Sens. 40, 110–122.